Check for updates

Synthesis of ternary oxide Zn₂GeO₄ nanowire networks and their deep ultraviolet detection properties

Xu Han, [ID] [abc] Shuanglong Feng, [bc] Yiming Zhao, [abc] Lei Li, [bc] Zhaoyao Zhan, [ID] *[bcd] Zhiyong Tao, [a] Yaxian Fan, *[a] Wenqiang Lu, [ID] *[abc] Wenbin Zuo [e] and Dejun Fu [e]

Ternary oxide Zn₂GeO₄ with a wide bandgap of 4.84 eV, as a candidate for fourth generation semiconductors, has attracted a great deal of attention for deep ultraviolet (DUV) photodetector applications, because it is expected to be blind to the UV-A/B band (290–400 nm) and only responsive to the UV-C band (200–290 nm). Here, we report on the synthesis of Zn₂GeO₄ nanowire (NW) networks by lower pressure chemical vapor deposition and investigate their corresponding DUV detection properties. We find that pure Zn₂GeO₄ NWs could be obtained at a growth pressure of 1 kPa. The DUV detection tests reveal that growth pressure exerts a significant effect on DUV detection performance. The Zn₂GeO₄ NW networks produced under 1 kPa show an excellent solar-blind photoresponsivity with fast rise and decay times ($t_{rise} \approx 0.17$ s and $t_{decay} \approx 0.14$ s).

1. Introduction

Recently, wide-bandgap metal oxide nanostructures have attracted extensive attention for potential application in next-generation electronics including transparent conductive electrodes, sensing elements, energy harvesting and storage devices, and optoelectronics.[1–10] Among them, UV detection, especially, solar-blind deep ultraviolet (DUV) photodetection is emerging as a hot topic because of their wide applications in commercial and military fields, including flame or engine monitoring, environmental and biological research, space technology, and missile launch.[11–18] To date, extensive attention has been paid to binary wide-bandgap materials for UV detection, such as ZnO,[19] SnO₂,[20] ZnS,[11–14] MnO₃ [21] and AlN.[22] However, much less effort has been devoted to more complex systems, such as ternary oxides, probably due to the difficulty with the preparation of high quality ternary nanostructures. Generally, ternary oxide systems are more chemically and thermally stable, and are more competitive candidates for deep UV detection due to their larger bandgap and hence higher

[a] School of Physics, Key Laboratory of InFiber Integrated Optics, Ministry of Education of China, Harbin Engineering University, Harbin 150001, China. E-mail: yxfan@hrbeu.edu.cn; wqlu@cigit.ac.cn

[b] Chongqing Key Laboratory of Multi-scale Manufacturing Technology, Chongqing Institute of Green and Intelligent Technology, Chinese Academy of Sciences, Chongqing 400714, China. E-mail: zhanhit@hotmail.com

[c] University of Chinese Academy of Sciences, Beijing, China

[d] School of Mechanical and Aerospace Engineering, Nanyang Technological University, 50 Nanyang Ave., 639798, Singapore

[e] Key Laboratory of Artificial Micro, and Nano-Materials of Ministry of Education, School of Physics and Technology, Wuhan University, Wuhan 430072, China

photon energy thresholds. Recently, several ternary oxides including Zn₂SnO₄, In₂Ge₂O₇, and ZnGa₂O₄ have been employed for DUV detection. Among these candidates, ternary oxide Zn₂GeO₄ has a wide bandgap of about 4.84 eV, which is expected to be blind to UV-A/B band (290–400 nm) and only responsive to UV-C band (200–290 nm).[5,9,10] The Zn₂GeO₄ nanostructures, especially Zn₂GeO₄ nanowires (NWs), have attracted a great deal of attention because of large specific surface area,[2,4,23] fast charge transport characteristics,[24] and high optical absorption. To utilize their full potential in DUV photodetection, Zn₂GeO₄ NWs should be facilely fabricated and integrated into DUV photodetectors (PDs) with fast response speed in a cost-effective manner. At the same time, there is a huge possibility in the field of wearable devices with further exploration on flexible substrate as well as self-powered photodetector.[25,26] Previously, we have proposed that the response speed of metal oxide NW-based UV PDs could be improved by directly growing entangled NW array grown on SiO₂ by chemical vapor deposition (CVD). The interconnections in NW array creates NW–NW junction barriers which dominate the inter-wire charge transport. The UV illumination induces fast tuning of NW–NW junction barrier height, which contributes to the enhanced response speed of the NW-array UV PDs. Thus the Zn₂GeO₄ NW networks should bear great advantages in terms of PDs fabrication and also response speed.

Usually, growth of Zn₂GeO₄ NWs is conducted under a very stringent condition (low pressure < 500 Pa, and high temperature ~ 1000 °C).[5,10] The effect of pressure on growth of Zn₂GeO₄ NWs and the corresponding solar blind UV detection properties have not been fully investigated. Generally, the growth rate of Zn₂GeO₄ NWs is proportional to the vapor pressure in the CVD
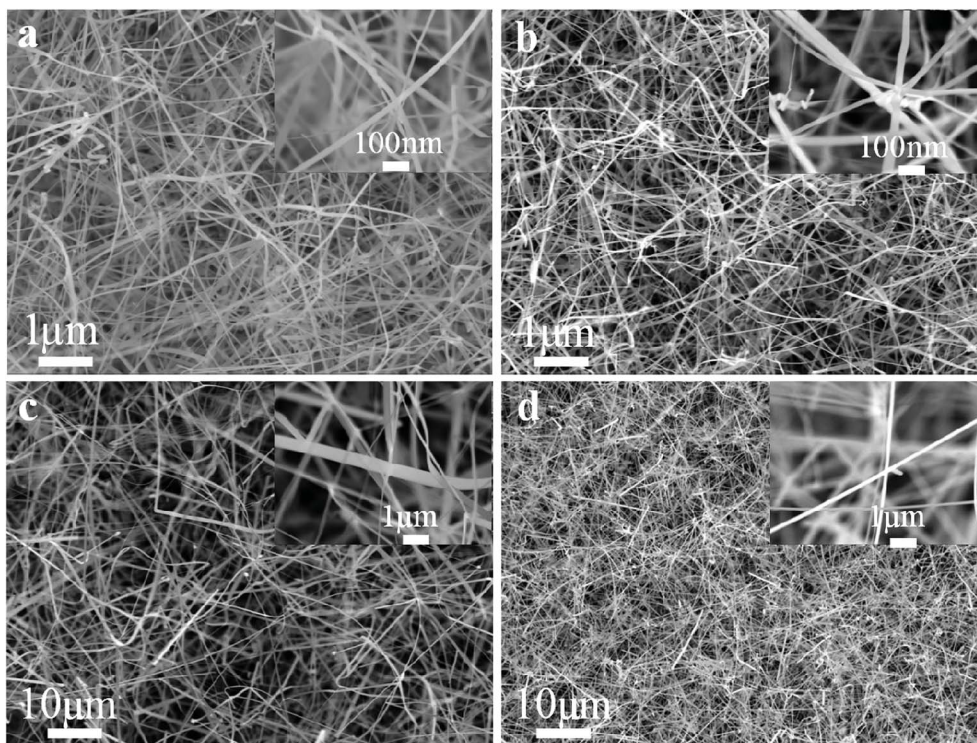
Fig. 1 SEM images of the as-grown Zn_2GeO_4 NW networks grown under different pressures at 960 °C for 15 min, the insets show the high magnification SEM images. (a) 0.5 kPa; (b) 1 kPa; (c) 2 kPa; (d) 5 kPa. The insets show the enlarged SEM images of the respective samples.

system. In addition, low vacuum level is also easy to achieve and maintain. Thus it would be desirable to grow high quality Zn_2GeO_4 NWs at a relatively higher pressure. In this paper, we report on synthesis of Zn_2GeO_4 NW networks at relatively higher pressure and investigate their DUV detection properties. We find that the pure Zn_2GeO_4 NWs could be only obtained at a growth pressure of 1 kPa or lower pressure; the higher pressure could lead to growth of Zn_2GeO_4 NW networks with impurities but at a higher growth rate. The DUV detection tests also reveal that growth pressure exerted a significant effect on DUV detection performance. The Zn_2GeO_4 NW networks produced under 1 kPa shows an excellent solar-blind photoresponsivity such as fast rise and decay times ($t_{rise} \approx 0.17$ s and $t_{decay} \approx 0.14$ s) justifying the potential of the Zn_2GeO_4 nanowires for solar-blind DUV detection.

2. Experimental

Zn_2GeO_4 nanowires were synthesized *via* a facile CVD method. 0.421 g mixture of ZnO, GeO_2, and diamond powders (molar ratio of 2 : 1 : 3) was loaded in a ceramic boat which is located at the center of quartz tube furnace. A piece of Si substrate (500 nm SiO_2/Si) coated with 3 nm Au films was covered just above the source materials. 100 standard cubic centimeter per minute (sccm) Ar was introduced into the chamber as carrier gas. The tube furnace was then heated to 960 °C within 68 min. Once the temperature reached 600 °C, 1.5 sccm oxygen was introduced into the furnace. To evaluate the effect of pressure on Zn_2GeO_4 NW networks growth, the pressure in the chamber

was set to 0.5 kPa, 1 kPa, 2 kPa, 5 kPa and 15 kPa, respectively. The furnace was kept at 960 °C for 15 min, and then the oxygen was switched off and the furnace was cooled naturally down to room temperature. After growth, a layer of white or gray materials were obtained on the SiO_2/Si substrates. The final products were characterized and analyzed by a SEM (JSM-7800F, JEOL) equipped with an EDX detector, XRD (D8 ADVANCE, BRUCKER), and a HRTEM (Tecnai G2-F20, FEI). The Raman spectra were collected on a Renishaw system excited by an argon laser of 488 nm wavelength.

The devices were fabricated according to processes reported in our previous works.[1,2,30] A two-end metal-semiconductor-metal structured Zn_2GeO_4 NW network DUV PD was prepared by applying silver paint onto Zn_2GeO_4 NW networks to form two silver electrodes with internal space around 8 mm and enough thickness. Electrical properties such as *I–V* curves and photoresponse performance were measured at room temperature on a PW-400 probe station system with a sourcemeter (4200-SCS, Keithley) and a 256 nm LED lamp (LDLS, EQ-1500) whose power is 1.76 mW cm^{-2}.

3. Results and discussion

The morphologies of the Zn_2GeO_4 NW networks synthesized at different pressures are shown in Fig. 1. The nanowires have a high density, as individual nanowires entangle with each other, which will be beneficial for UV photodetector fabrication. The insets to Fig. 1 show enlarged images of the as-prepared products. Fig. 1a shows the Zn_2GeO_4 NW networks
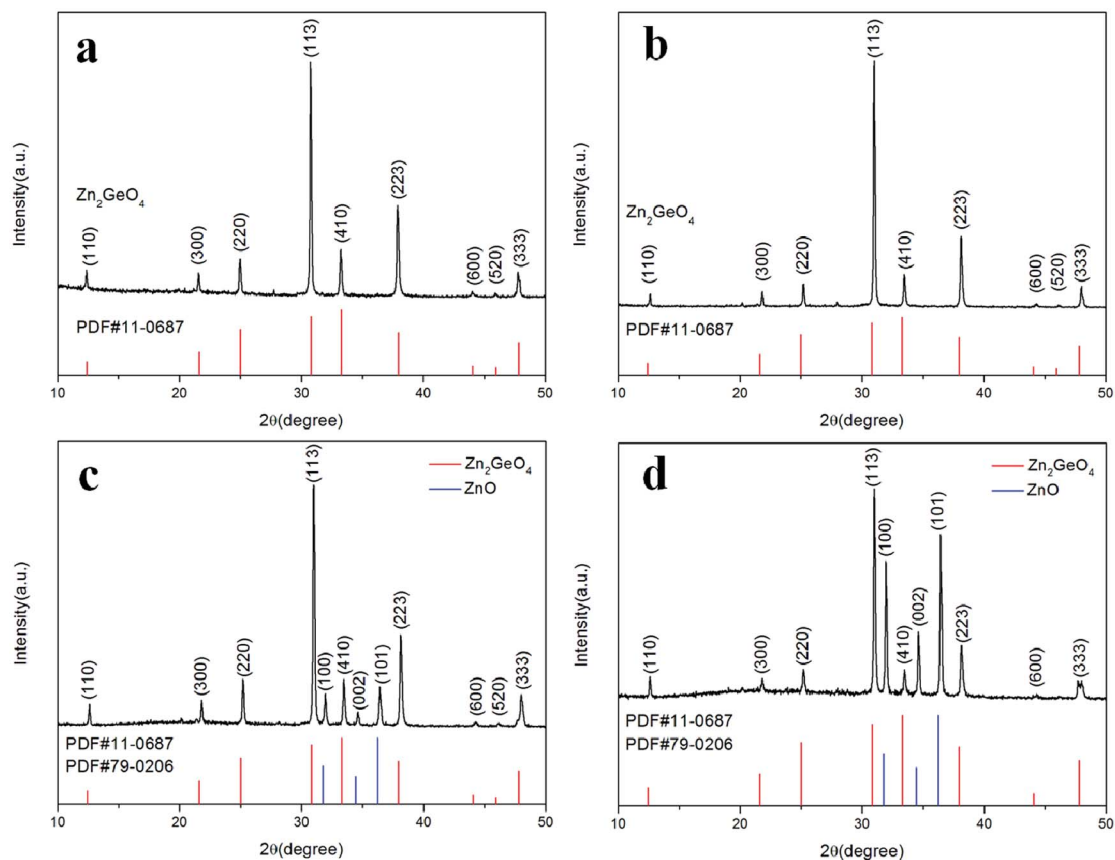
Fig. 2   XRD patterns of Zn_2GeO_4 NWs grown at different pressures. (a) 0.5 kPa; (b) 1 kPa; (c) 2 kPa; and (d) 5 kPa.

synthesized at 0.5 kPa, the NWs are about 40–90 nm in diameter (seen in the inset of Fig. 1a). The SEM image in Fig. 1b shows that the Zn_2GeO_4 NWs grown at 1 kPa have an average diameter of around 130 nm. The NW sample grown at 2 kPa could reach 200 nm in diameter (Fig. 1c). By further increasing the growth pressure to 5 kPa, we obtained Zn_2GeO_4 NWs with an average diameter of 300 nm. It is obvious that the diameter of NWs increases with the growth pressure if the other growth conditions are kept unchanged. The effect of growth pressure on the diameter is caused by the change in supersaturation. The vapor of Zn and Ge is determined by the local temperature, so the rate of producing the Zn and Ge vapor it can be assumed to be
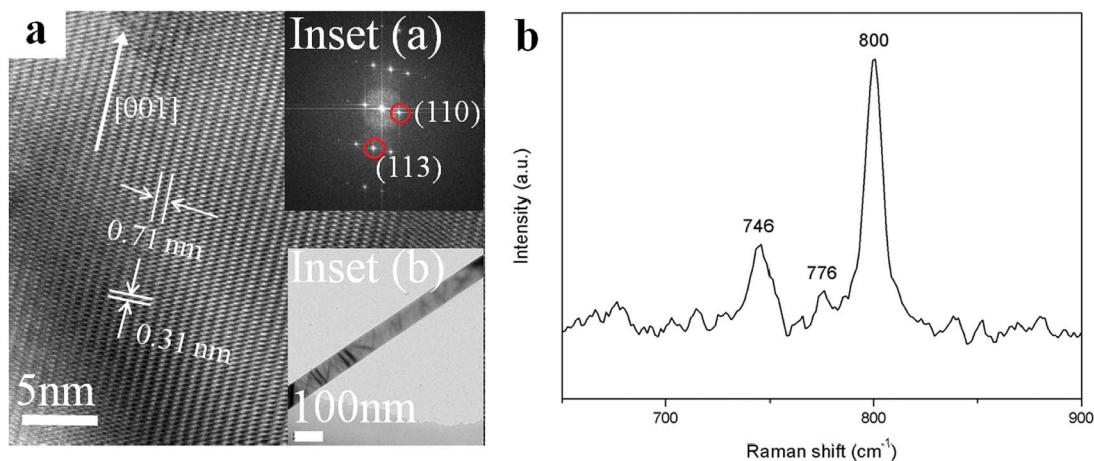

Fig. 3   (a) HRTEM image of single Zn_2GeO_4 NWs grown at pressure of 1 kPa. Inset (a) is the corresponding SAED pattern, indicating that the growth direction of nanowire is [001]. Inset (b) shows the low magnification TEM image. (b) Raman spectrum of the Zn_2GeO_4 NWs grown at pressure of 1 kPa.
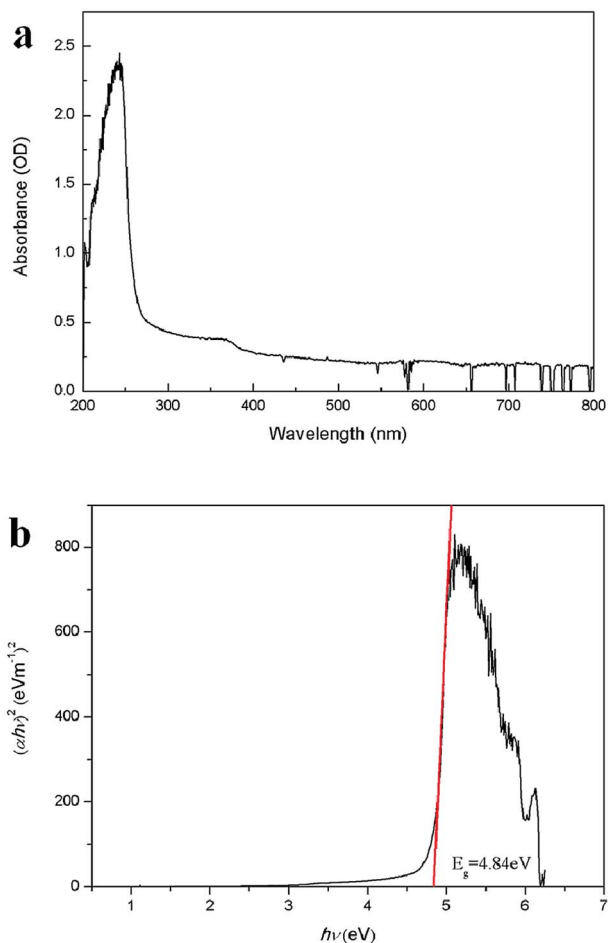
Fig. 4 (a) The absorption spectrum of Zn_2GeO_4 NWs. (b) Tauc's plot of $(\alpha h\nu)^2$ as a function of photon energy $h\nu$ for Zn_2GeO_4 NWs.

a constant under different chamber pressures. As a result, the partial pressure of the Zn and Ge vapor decreases when the total system pressure rise.[31] It implies that the supersaturation level gradually decreases with the increase of growth pressure. Thus, at low growth pressure, the growth condition with high supersaturation enhanced the heterogeneous nucleation, which results in high density of nucleation and formation of smaller diameter of nanowires. In contrast, at high growth pressure, the low supersaturation of growth condition strengthened the homogeneous nucleation from vapor phase, which induces the formation of larger diameter and the multifaceted tripod structures of nanowires.[32]

The effect of growth pressure on the product quality and purity was investigated by XRD technique, as shown in Fig. 2. As seen in Fig. 2a and b, when the growth pressure are 0.5 kPa and 1 kPa, the diffraction peak positions are in good agreement with the rhombohedral crystal of Zn_2GeO_4 phase (JCPDS card no. 11-0687). However, once the growth pressure is higher than 2 kPa, other diffraction peaks would appear and could be indexed to the diffraction peaks of ZnO (JCPDS card no. 79-0206), suggesting that ZnO is easier to grow along with Zn_2GeO_4 at higher pressure. This also suggests that the pure Zn_2GeO_4 NWs could only be obtained at a relatively lower growth pressure.

Fine structures of individual Zn_2GeO_4 nanowires were then characterized using HRTEM. The low magnification TEM images of Zn_2GeO_4 NWs synthesized under pressure of 1 kPa are shown in Fig. 3a. The corresponding inserts give HRTEM images recorded along the $[1\bar{1}0]$ zone axis. Specifically, the measured lattice distances was calculated to be about 0.71 nm and 0.31 nm which can be assigned to separations of the adjacent (110) and (113) planes, respectively. From the selected area electron diffraction (SAED) pattern of inset (a), it can be deduced that the preferred growth direction of a single nanowire is along the [001] direction.[15] Combined the SAED and the high-resolution TEM (HRTEM) data, the formation of single crystalline nanowire could be confirmed readily. Simultaneously, the HRTEM also documented the high single-crystal quality of the samples, no defects were seen. It is obviously the excellent quality and high aspect ratios make the as-synthesized Zn_2GeO_4 nanowires become promising candidates for optoelectronic devices.

Fig. 3b shows the local atomic structure of the Zn_2GeO_4 nanowires which was further investigated by Raman spectroscopy. The most prominent peak around 800 cm^{-1} which corresponds to the stretching vibration of GeO_4 tetrahedra could be observed from the plot. The peaks at 746 and 776 cm^{-1} could be attributed to the symmetric and asymmetric stretching vibrations of Ge–O–Zn bonds, respectively.[28,29] According to the previous report, the peak around 754 cm^{-1} was usually associated with oxygen defects in Zn_2GeO_4.[30] However, it is visible this peak was not detectable in as-synthesized nanowires, indicating that there are negligible oxygen defects in the present Zn_2GeO_4 nanowires. It also suggested a high-quality crystal structure of the final products.

Fig. 4a shows the absorption spectrum of Zn_2GeO_4 nanowires on quartz substrate. The absorption peak of the nanowires can be seen clearly, and the peak position of the Zn_2GeO_4 nanowires locates at about 243 nm, indicating that the incorporation of germanium oxide makes the absorption spectrum of shift to deep ultraviolet. This observation reveals that the Zn_2GeO_4 NWs exhibit high wavelength selectivity in the UV-C region, as compared with the binary oxides, such as ZnO and SnO_2.[30–35] The bandgap of the Zn_2GeO_4 nanowires could also been obtained by fitting the absorbance with respect to the photon energy, as shown in Fig. 4b. The bandgap obtained from Tauc plot is 4.84 eV, which is in good agreement with the reported results.[30]

To examine the response time of the Zn_2GeO_4 nanowires UV photodetector, a LED lamp with wavelength of 256 nm and energy density of 1.76 mW cm^{-2} was used as a light source. The time-dependent photocurrent at 8 V bias with multiple UV on/off cycles was measured at room temperature, in which both the "on" and "off" times of the UV illumination were 20 s. It is well-known that oxygen molecules absorbed on the surface of Zn_2GeO_4 act as electron acceptors to form O_2^- by capturing free electrons from the surface in dark, creating a low conductive depletion layer near the Zn_2GeO_4 surface.[1,2,27,28] Upon UV illumination, the photogenerated holes in Zn_2GeO_4 migrate to the surface and neutralize the O_2^- ions, while the unpaired electrons significantly enhance the conductivity of the sample. The
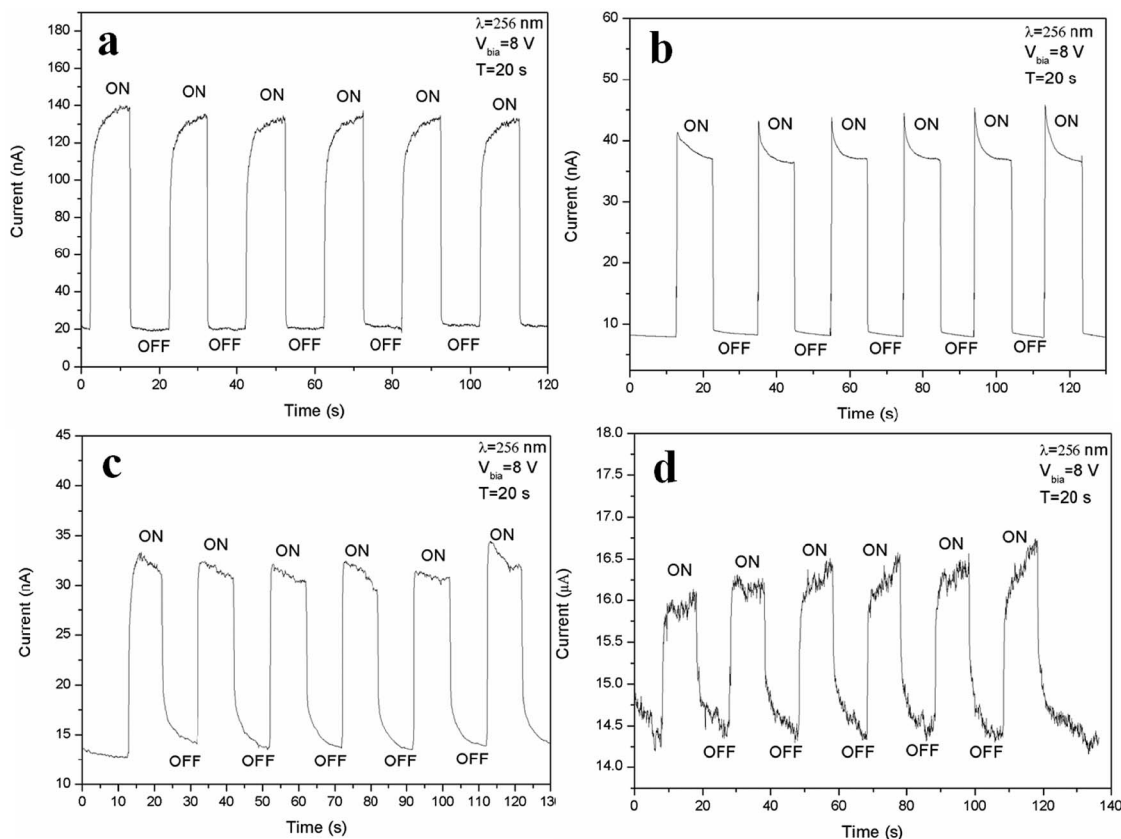
Fig. 5 Time-resolved rise and decay of photocurrent with UV illumination on and off periods of 20 s under a bias of 8 V of Zn_2GeO_4 NW networks grown under pressures of 0.5 kPa (a), 1 kPa (b), 2 kPa (c), and 5 kPa (d).

photoelectric characteristic images of Zn_2GeO_4 nanowire networks under different pressures (0.5–5 kPa) with a period of 20 s are shown in Fig. 5. As shown in Fig. 5a, upon UV illumination, the current would first rapidly ramp to 130 nA from the dark current, then it increases tardily to 140 nA, and as UV illumination is off, the current would promptly fall to the original level. From Fig. 5b, it can be seen that current dramatically expands from the dark current to 44 nA, which is associated to UV illumination, and then it gradually goes down to around 37 nA, and when UV illumination is off, the current would swiftly decline to around the original level. It is evident that upon UV illumination, the current would first quickly change to 31 nA from the dark current, and then decrease gently to 30 nA, and as UV illumination is off, the current would first speedily descend to 17 nA and then slowly decay to around the dark current from Fig. 5c. As shown in Fig. 5d, upon UV illumination, the current would first drastically go up to 16 nA from the dark current, followed by a slow rise to 16.5 nA, and as UV illumination is off, the current would first sharply reduce to 15 nA and then drop to around the original level by inches. It is clear that by switching on and off the electron beam, the devices run with good repeatability with fast response (<1 s).

It is obvious that the device (under a bias of 8 V) shows a good stability, as well as fast rise and decay times, as illustrated in Fig. 6. If we define t_r and t_d as the times required for the current to increase from 10% to 90% of the peak value or *vice versa*,[15] then the response and recovery time of the

photodetectors prepared from Zn_2GeO_4 NWs grown at 0.5 kPa can be calculated to be 1.68 s and 0.11 s, respectively. From the curve, it can be seen that the typical response time of the Zn_2GeO_4 NW network UV PD with nanowires synthesized under 1 kPa is about 0.17 s and it has a steep falling edge, giving a recovery time of 0.14 s. The measured t_r and t_d of the Zn_2GeO_4 NW network UV PD made of NWs grown at 2 kPa can be deduced to be 0.11 s and 2.48 s, respectively. On the contrary, the device fabricated from Zn_2GeO_4 NW synthesized under 5 kPa has the response and recovery time of $t_r = 0.94$ s and $t_d = 3.15$ s respectively.

It is found that the rise process (0.17 s) of the Zn_2GeO_4 NW network UV PD with nanowires synthesized under 1 kPa is much faster than that of Zn_2GeO_4 NW PD obtained from nanowires grown at 0.5 kPa (1.68 s) and 5 kPa (0.94 s), while the rise stage of Zn_2GeO_4 NW network PD prepared from NWs produced at 1 kPa is also comparable with that of the device with nanowires grown at 2 kPa (0.11 s).[31] Likewise, the resetting process of the PDs with NWs grown 1 kPa (0.14 s) is much faster than the devices corresponding to 2 kPa (2.84 s) and 5 kPa (3.15 s), while the decay stage of the Zn_2GeO_4 NW PD produced at 1 kPa is also comparable with that of NW device grown at 0.5 kPa (0.11 s). This is much better than most reported PDs based on Zn_2GeO_4 nanostructures, as shown in Table 1.[34]

To determine the other aspects of sensing performance, the responsivity (R), external quantum efficiency (EQE) and detectivity (D*) corresponding to the detectors of different growth
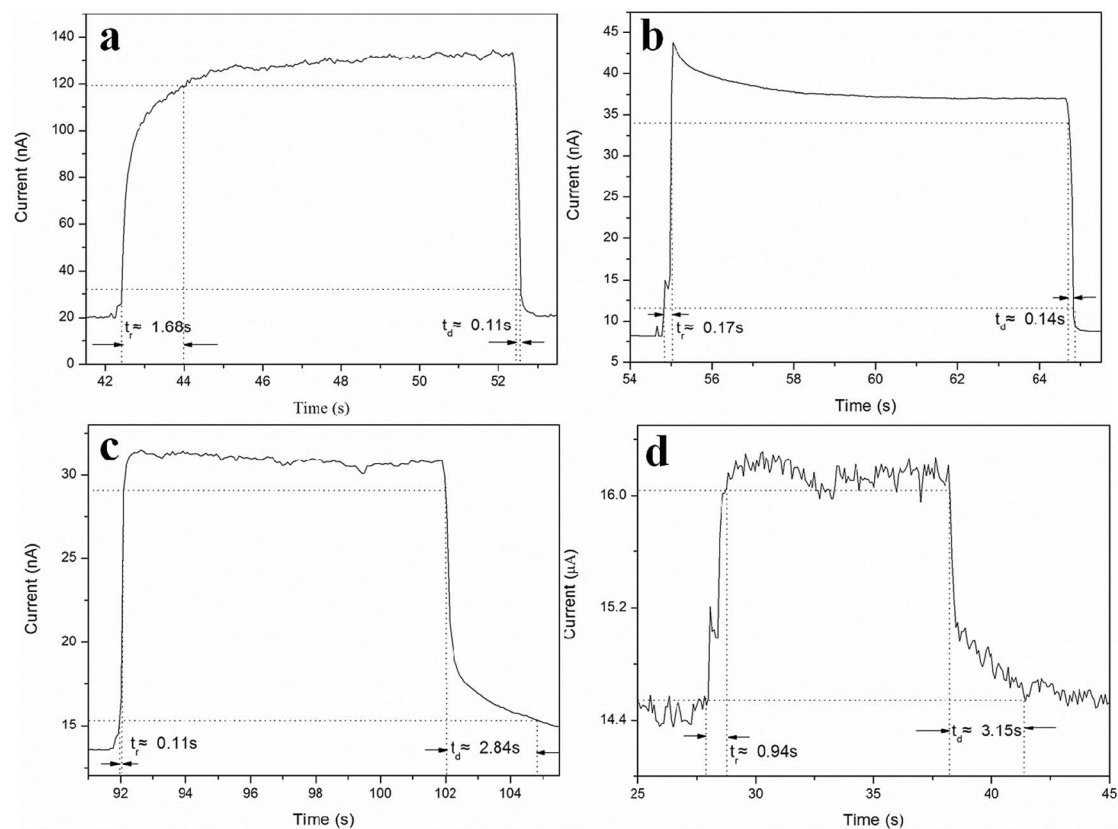
Fig. 6 Enlarged view of typical rise and decay curves for Zn_2GeO_4 NW network PD synthesized at different pressures with and without UV illumination. (a) 0.5 kPa; (b) 1 kPa; (c) 2 kPa; and (d) 5 kPa.

Table 1 Comparison of Zn_2GeO_4 and other ternary oxide nanostructures based photodetector parameters between this work and the previous reports

Photodetectors	Bias (V)	UV light (nm) and power density (mW cm^{-2})	Rise time (s)	Decay time (s)	Ref.
Zn_2GeO_4 NW	3	$\lambda = 254, P = /$	0.6	1.5	9
Zn_2GeO_4 NW mats	20	$\lambda = 254, P = 0.2$	0.3	0.2	30
Zn_2GeO_4 NW	8	$\lambda = 245, P = 0.05$	12	0.6	37
$In_2Ge_2O_7$ NW mats	20	$\lambda = 254, P = 0.85$	15	<1	38
Zn_2GeO_4 NW	3	$\lambda = 254, P = 0.85$	3	<1	38
$ZnGa_2O_4$ NW	5	$\lambda = 350, P = 0.53$	15	10	39
Zn_2GeO_4 NW networks	8	$\lambda = 256, P = 1.76$	0.17	0.14	This work

pressures were calculated. The responsivity of the Zn_2GeO_4 nanowires UV photodetectors is defined as the ratio of the response current to the illumination power on photodetector as given by:[15,33,40]

$$R = \frac{\Delta I}{PS} \qquad (1)$$

where ΔI is the response current (current difference between photocurrent and dark current), P is the incident UV power density, and S is the active device area. In this experiment, the UV illumination power density is 1.76 mW cm^{-2}, the active area is 4 mm^2. The external quantum efficiency (EQE) is given by the following relation:

$$EQE = \frac{hcR}{e\lambda} \qquad (2)$$

where h is the Plank's constant and e is the absolute value of electron charge (1.6×10^{-19} C), λ is the wavelength of incident light, and the wavelength is 256 nm. Furthermore, if we consider the shot noise as the major portion of the total noise, detectivity (D^*) in units of jones, an index to evaluate the photoresponse, can be expressed as following equation:[15,26,40–42]

$$D^* = \frac{RS^{\frac{1}{2}}}{(2eI_d)^{\frac{1}{2}}} \qquad (3)$$

where I_d is the dark current, S is the effective area of the detectors and e is the electron charge. The responsivity, external quantum efficiency and detectivity of various photodetectors were listed in the Table 2.

Table 2 The parameters of responsivity, external quantum efficiency and detectivity corresponding to PDs of different growth pressures

Photodetectors of different growth pressures	Responsivity (R)	External quantum efficiency (EQE)	Detectivity (D^*)
0.5 kPa	1.7×10^{-3} A W^{-1}	0.82%	4.25×10^9 jones
1 kPa	5.11×10^{-4} A W^{-1}	0.25%	2.03×10^9 jones
2 kPa	2.98×10^{-4} A W^{-1}	0.15%	9.22×10^8 jones
5 kPa	4.26×10^{-5} A W^{-1}	0.02%	1.27×10^8 jones

The entanglement between Zn_2GeO_4 NWs is beneficial to response speed through the mechanism of Schottky barriers at the junctions between the interconnected Zn_2GeO_4 NWs. On the other hand, the entanglement in Zn_2GeO_4 NWs usually formed in high density Zn_2GeO_4 NWs at the cost of photo-to-dark current ratio.[34] There are two main factors for high dark current. First, only very few Zn_2GeO_4 NWs on the top of Zn_2GeO_4 NW networks could absorb and be excited by UV illumination. Second, there would form a Zn_2GeO_4 film on the substrate as the reaction proceeds and contribute to the high dark current.[34]

While the structure of interconnection of Zn_2GeO_4 NWs has fast response time, the electrical signal of the material is weak, which affects the value of the responsivity, external quantum efficiency and detectivity of photodetectors.

Fig. 7 shows the schematic diagram depicting the carrier generation and transportation processes in the Zn_2GeO_4 NW network devices. It is well accepted that the processes of oxygen adsorption and desorption corresponding to the UV response and recovery are associated with the photogeneration of free carriers.[30,35,36,38–43] In ambient conditions, oxygen molecules
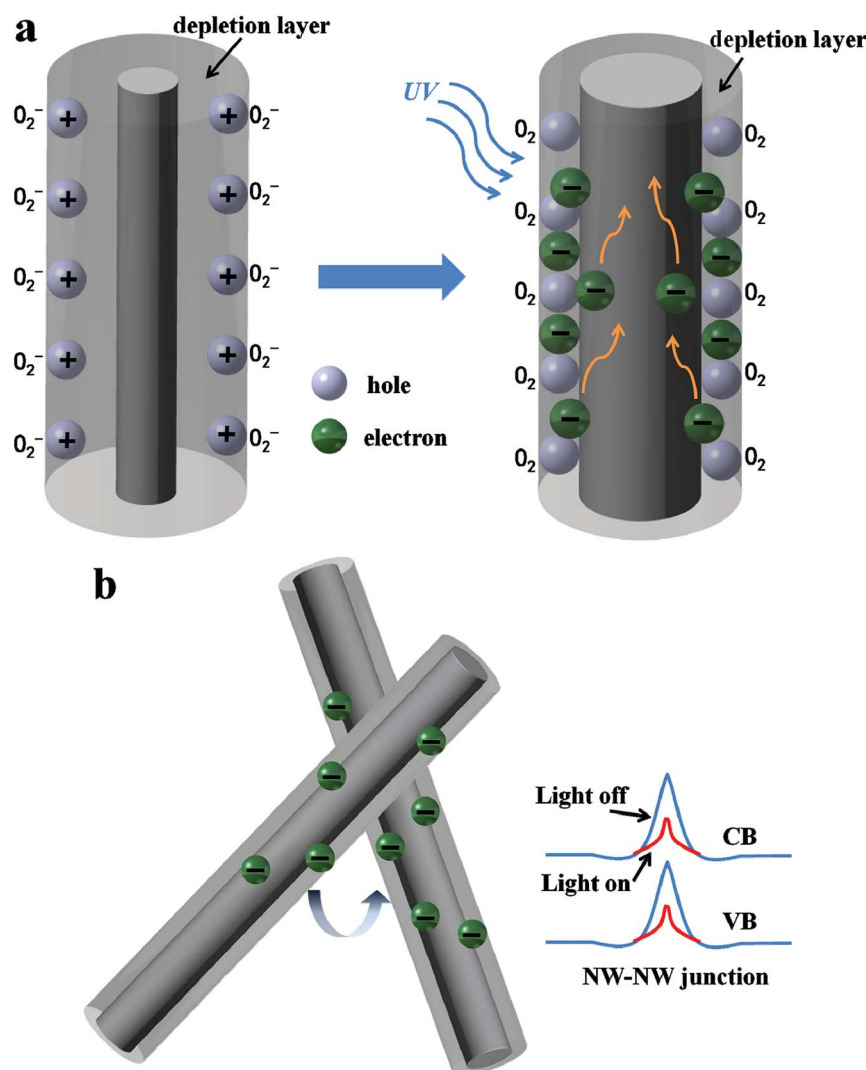
Fig. 7 Schematic of the carrier generation and NW–NW junction barrier for electron transfer in the network device. (a) Carrier generation in a single Zn_2GeO_4 NW; (b) carrier generation and transport in Zn_2GeO_4 NW.

would adsorb on the surface of Zn_2GeO_4 NW to form O_2^- by capturing free electrons from NW surface through O_2 (g) + $e^- \rightarrow O_2^-$ (ad), creating a lowly conductive surface depletion layer, as shown in Fig. 6a. Under the UV irradiation, the electron–hole pairs are generated by directly exciting electrons from the valence band to conduction band, which increase carrier density significantly in the NWs. The photon-generated holes would migrate to the surface and discharge the adsorbed oxygen ions through O_2^- (ad) + $h^+ \rightarrow O_2$ (g), resulting in a reduction in the depletion barrier thickness. The increase in carrier concentration and oxygen desorption caused by hole-trapping process contribute to an apparent enhancement of conductance in the NW networks.[30–34] As the UV illumination is turned off, holes recombine with electrons, meanwhile oxygen re-absorb on Zn_2GeO_4 NW surface by capturing electrons returning the device to initial low conductivity state.

In addition to the same photoconductive mechanism of photogeneration of free carriers, compared with single NW PD, network devices have another unique conducting mechanism that is the transport of carriers across the interface between neighboring NWs. As Fig. 6b illustrates, the resistance of two crossed NWs was dominated by the NW–NW junction barrier, rather than the resistances of the NW themselves.[44,45] In the Zn_2GeO_4 NW PD, electrons must overcome the NW–NW junction barrier when tunneling from one NW to another as shown in Fig. 6b. It is reported that the electron-transfer barrier originates from the surface depletion layers and the depletion layer would be narrowed upon UV illumination on account of the increase of carrier density, which is equivalent to a lowering of the effective barrier height.[30–34] It makes electrons more likely to transport in the networks upon UV irradiation and hence resulting in the increment of current, as illustrated in Fig. 4.

Compared with the previously reported devices with slow response and recovery time,[36,39,43–48] the fast recovery time 0.14 s for our Zn_2GeO_4 NW photodetectors can be attributed to the NW–NW junction barrier dominated conductance. Typically, because it needs a long time for the oxygen diffusion and re-adsorption to deplete the NW channel, the NW conductance is still higher than its initial value within a short period upon turning off the UV light.[30,43,46–48] For the NW network structures, the depletion barrier can be analogous to two back-to-back Schottky barriers, as the UV light is switched on, which is much lower in the effective barrier height due to the greatly incremental carrier density. The dominate role of the junction barrier would cause a current decay almost approaching its initial value within a short period for our devices. The modulation of barrier height induced by irradiation is typically much faster than the oxygen diffusion process on the order of several minutes or hours. This paper demonstrates that the response and recovery time can be enhanced by using NW networks with NW–NW barrier dominated conductance. It can be seen that apart from no requirement for intense and expensive lithography processes, the simple and feasible preparation technics also allows potential large-scale device fabrication.

4. Conclusion

In conclusion, we have prepared wide-bandgap Zn_2GeO_4 NW networks by CVD at lower pressures (0.5–5 kPa) and investigated their corresponding DUV detection performance. We found that the pure Zn_2GeO_4 NWs could be obtained at 1 kPa or lower pressure. The Zn_2GeO_4 NW networks produced under 1 kPa exhibited efficient response for UV photodetection. The network devices showed response and recovery time of 0.17 s and 0.14 s, respectively, which can be attributed to the NW–NW junction barrier dominant conductance. The large bandgap 4.84 eV makes the NW materials promising for UV-C detection with high wavelength selectivity. The network-enabled fast response and recovery time as well as facile fabrication processes may also be extended to other ternary metal oxide nanomaterials.

Conflicts of interest

There are no conflicts to declare.

Acknowledgements

References

1 H. Kind, H. Q. Yan, B. Messer, M. Law and P. D. Yang, *Adv. Mater.*, 2002, **14**, 158–160.

2 Z. R. Dai, Z. W. Pan and Z. L. Wang, *Adv. Funct. Mater.*, 2003, **13**, 9–24.

3 S. Xu, Y. Qin, C. Xu, Y. Wei, R. Yang and Z. L. Wang, *Nat. Nanotechnol.*, 2010, **5**, 366–373.

4 J. Bao, M. A. Zimmler, F. Capasso, X. Wang and Z. Ren, *Nano Lett.*, 2006, **6**, 1719–1722.

5 S. J. Chang, T. J. Hsueh, I. C. Chen and B. R. Huang, *Nanotechnology*, 2008, **19**, 175502–175506.

6 J. Zhou, Y. Gu, Y. Hu, W. Mai, P. H. Yeh, G. Bao, A. K. Sood, D. L. Polla and Z. L. Wang, *Appl. Phys. Lett.*, 2009, **94**, 191103.

7 C. Y. Hsieh, M. L. Lu, J. Y. Chen, Y. T. Chen, Y. F. Chen, W. Y. Shih and W. H. Shih, *Nanotechnology*, 2012, **23**, 355201–355205.

8 S. Liang, H. Sheng, Y. Liu, Z. Huo, Y. Lu and H. Shen, *J. Cryst. Growth*, 2001, **225**, 110–113.

9 C. H. Liao, C. W. Huang, J. Y. Chen, C. H. Chiu, T. C. Tsai, K. C. Lu, M. Y. Lu and W. W. Wu, *J. Phys. Chem. C*, 2014, **118**, 8194–8199.

10 Q. Zhang, J. S. Jie, S. L. Diao, Z. V. Shao, Q. Zhang, L. Wang, W. Deng, W. D. Hu, H. Xia, X. D. Yuan and S. T. Lee, *ACS Nano*, 2015, **9**, 1561–1570.

11 R. J. Zou, Z. Y. Zhang, Q. Liu, J. Q. Hu, L. W. Sang, M. Y. Liao and W. J. Zhang, *Small*, 2014, **10**, 1848–1856.

12 X. Fang, Y. Bando, M. Liao, T. Zhai, U. K. Gautam, L. Li, Y. Koide and D. Golberg, *Adv. Funct. Mater.*, 2010, **20**, 500–508.

13 Y. Li, T. Tokizono, M. Liao, M. Zhong, Y. Koide, I. Yamada and J. J. Delaunay, *Adv. Funct. Mater.*, 2010, **20**, 3972–3978.

14 T. Zhai, L. Li, X. Wang, X. Fang, Y. Bando and D. Golberg, *Adv. Funct. Mater.*, 2010, **20**, 4233–4248.

15 X. Zhou, Q. Zhang, L. Gan, X. Li, H. Li, Y. Zhang, D. Golberg and T. Zhai, *Adv. Funct. Mater.*, 2016, **26**, 704–712.

16 Z. Zhang, Q. L. Liao, Y. H. Yu, X. D. Wang and Y. Zhang, *Nano Energy*, 2014, **9**, 237–244.

17 X. K. Zhang, Q. L. Liao, S. Liu, Z. Kang, Z. Zhang, J. L. Du, F. Li, S. H. Zhang, J. K. Xiao, B. S. Liu, Y. Ou, X. Z. Liu, L. Gu and Y. Zhang, *Nat. Commun.*, 2017, **8**, 15881.

18 J. Z. Song and H. B. Zeng, *Angew. Chem., Int. Ed.*, 2015, **54**, 9760–9774.

19 S. Majety, J. Li, X. K. Cao, R. Dahal, B. N. Pantha, J. Y. Lin and H. X. Jiang, *Appl. Phys. Lett.*, 2012, **100**, 061121.

20 S. Ohmagari and T. Yoshitake, *Appl. Phys. Express*, 2012, **5**, 5202.

21 J. Zhou, Y. Gu, Y. Hu, W. Mai, P. H. Yeh, G. Bao, A. K. Sood, D. L. Polla and Z. L. Wang, *Appl. Phys. Lett.*, 2009, **94**, 191103.

22 C. Y. Hsieh, M. L. Lu, J. Y. Chen, Y. T. Chen, Y. F. Chen, W. Y. Shih and W. H. Shih, *Nanotechnology*, 2012, **23**, 355201–355205.

23 S. Mehrabani, P. Kwong, M. Gupta and A. M. Armani, *Appl. Phys. Lett.*, 2013, **102**, 241101.

24 X. Pan, X. Liu, A. Bermak and Z. Fan, *ACS Nano*, 2013, **7**, 9318–9324.

25 J. Z. Song, J. H. Li, J. Y. Xu and H. B. Zeng, *Nano Lett.*, 2014, **14**, 6298–6305.

26 Y. Zhang, Y. Yang, Y. S. Gua, X. Q. Yan, Q. L. Liao, P. F. Li, Z. Zhang and Z. Z. Wang, *Nano Energy*, 2015, **14**, 30–48.

27 L. Xu, X. Li, Z. Zhan, L. Wang, S. Feng, X. Chai, W. Lu, J. Shen, Z. Weng and J. Sun, *ACS Appl. Mater. Interfaces*, 2015, **7**, 20264–20271.

28 X. Q. Liao, X. Q. Yan, P. Lin, S. G. Lu, Y. Tian and Y. Zhang, *ACS Appl. Mater. Interfaces*, 2015, **7**, 1602–1607.

29 X. Lang, A. Hirata, T. Fujita and M. Chen, *Nat. Nanotechnol.*, 2011, **6**, 232–236.

30 C. Yan, N. Singh and P. S. Lee, *Appl. Phys. Lett.*, 2010, **96**, 053108.

31 J. H. Song, X. D. Wang, E. Riedo and Z. L. Wang, *J. Phys. Chem. B*, 2005, **109**, 9869–9872.

32 E. S. Babu, S. J. Kim, J. H. Song and S. K. Hong, *Chem. Phys. Lett.*, 2016, **658**, 182–187.

33 Z. Zhan, L. Xu, J. An, H. Du, Z. Weng and W. Lu, *Adv. Eng. Mater.*, 2017, **19**, 1700101.

34 L. Li, H. Jiang, X. Han, Z. Zhan, H. Du, W. Lu, Z. Li, Z. Tao and Y. Fan, *Ceram. Int.*, 2017, **43**, 15978–15985.

35 Z. Q. Liu, D. H. Zhang, S. Han, C. Li, T. Tang, W. Jin, X. L. Liu, B. Lei and C. W. Zhou, *Adv. Mater.*, 2003, **15**, 1754–1757.

36 C. Soci, A. Zhang, B. Xiang, S. A. Dayeh, D. P. R. Aplin, J. Park, X. Y. Bao, Y. H. Lo and D. Wang, *Nano Lett.*, 2007, **7**, 1003–1009.

37 C. Li, Y. Bando, M. Y. Liao, Y. Koide and D. Golberg, *Appl. Phys. Lett.*, 2010, **97**, 161102.

38 Z. Liu, H. T. Huang, B. Liang, X. F. Wang, Z. R. Wang, D. Chen and G. Z. Shen, *Opt. Express*, 2012, **20**, 2982–2991.

39 Z. Lou, L. D. Li and G. Z. Shen, *Nano Res.*, 2015, **8**, 2162–2169.

40 S. L. Wang, Y. S. Zou, Q. S. Shan, J. Xue, Y. H. Dong, Y. Gu and J. Z. Song, *RSC Adv.*, 2018, **8**, 33666–33673.

41 H. Kind, H. Q. Yan, B. Messer, M. Law and P. D. Yang, *Adv. Mater.*, 2002, **14**, 158–160.

42 Y. H. Dong, Y. Gu, Y. S. Zou, J. Z. Song, L. M. Xu, J. H. Li, J. Xue, X. M. Li and H. B. Zeng, *Small*, 2016, **12**, 5622–5632.

43 J. Zhou, Y. D. Gu, Y. F. Hu, W. J. Mai, P. H. Yeh, G. Bao, A. K. Sood, D. L. Polla and Z. L. Wang, *Appl. Phys. Lett.*, 2009, **94**, 191103.

44 X. F. Duan, Y. Huang, Y. Cui, J. F. Wang and C. M. Lieber, *Nature*, 2001, **409**, 66–69.

45 Y. Cui and C. M. Lieber, *Science*, 2001, **291**, 851–853.

46 A. Umar, B. K. Kim, J. J. Kim and Y. B. Hahn, *Nanotechnology*, 2007, **18**, 175606.

47 S. W. Lee, M. C. Jeong, J. M. Myoung, G. S. Chae and I. J. Chung, *Appl. Phys. Lett.*, 2007, **90**, 133115.

48 G. Lubberts, B. C. Burkey, H. K. Bucher and E. L. Wolf, *J. Appl. Phys.*, 1973, **45**, 92–95.